Modeling the population effects of escape mutations in SARS-CoV-2 to guide vaccination strategies

James S. Koopman [a,*], Carl P. Simon [a], Wayne M. Getz [b,c], Richard Salter [c,d]

[a] *University of Michigan, United States*
[b] *University of California, Berkeley, United States*
[c] *Numerus*
[d] *Oberlin College, United States*

A B S T R A C T

SARS-Cov-2 escape mutations (EM) have been detected and are spreading. Vaccines may need adjustment to respond to these or future mutations. We designed a population level model integrating both waning immunity and EM. We also designed a set of criteria for elaborating and fitting this model to cross-neutralization and other data with a goal of minimizing vaccine decision errors. We formulated four related models. These differ regarding which strains can drift to escape immunity in the host when that immunity was elicited by different strains. Across changing waning and escape mutation parameter values, these model variations led to patterns where: 1) EM are rare in the first epidemic, 2) rebound outbreaks after the first outbreak are accelerated by increasing waning and by increasing drifting, 3) the long term endemic level of infection is determined mostly by waning rates with small effects of the drifting parameter, 4) EM caused loss of vaccine effectiveness, and under some conditions: vaccines induced EM that caused higher levels of infection with vaccines than without them. The differences and similarities across the four models suggest paths for developing models specifying the epitopes where EM act. This model provides a base on which to construct epitope specific evolutionary models using new high-throughput assay data from population samples to guide vaccine decisions.

1. Introduction: The nature of the problem we address

SARS-CoV-2 has generated the most devastating pandemic in a century. Many aspects of SARS-CoV-2 dynamics remain insufficiently understood, including the risks of and reasons for the reinfections. These might arise either because of 1) waning of immunity, or 2) escape mutation drifting, in which the virus evolves to escape immunity stimulated by prior infections or vaccines. How these two factors interact with each other has not been previously described. Understanding the dynamics of possible interactions between these causes of reinfection could provide insights into how SARS-CoV-2 could evolve.

Endemic human coronaviruses provide hints about the future course of SARS-CoV-2. For such viruses, reinfection is common in all age groups with an average time to reinfection less than three years for the two endemic beta coronaviruses (Petrie et al. 2021). But how long it took those beta coronaviruses to settle into their endemic patterns and what drove that process is unknown. Exploring models of the process of going from pandemic to endemic patterns is one way to develop theory about

that transition. (Kissler et al. 2020) made such model explorations as did (Lavine et al., 2021). But neither of these efforts formulated the processes that drove evolution through transmission enhancing or immune escape mutations.

In the current SARS-CoV-2 epidemic, transmission increasing mutations were documented early on, but no variants with suspected escape mutations emerged during most of the first year. Subsequently, rapid accumulation and wide dissemination of these mutations (Harvey et al. 2021) have occurred. Observations of such mutations and how they relate to variants of concern are accumulating. This has generated new theories about what is driving variant emergence (Harvey et al. 2021). The need for models to integrate all this new knowledge into broader dynamic models is acknowledged in (Harvey et al. 2021). Such models could be especially valuable for making decisions about what mutations to include in vaccines. It is increasingly seeming like modifications of the early SARS-CoV-2 vaccines will be needed.

For influenza vaccine decisions, the question to be answered by models is which possible strains currently known to be circulating

should be chosen for inclusion in the next vaccine. Extensive phylogenetic data, cross-neutralization assays, and a little transmission system theory provide the basis for decisions (Huddleston et al. 2020). But for SARS-CoV-2, new approaches like mRNA vaccines along with extensive new data, theory, and laboratory methods could provide the basis for choosing which mutations to include rather than which strains. Models of processes by which mutations arise and spread are needed for that approach. We begin here with the exploration of models that integrate both waning and escape mutation drifting.

2. Methods: How we addressed this problem

We formulate a model with both waning of immunity across multiple levels and mutations that are captured as strain switches. The mutations could manifest both immune escape and transmission enhancement. In this paper, we only address escape mutations. We believe this is the first model to examine the interactions between waning and drifting in continuous time. (Andreasen 2003), presented an influenza model with both elements but with escape mutations occurring only between epidemic seasons.

Our model is an ordinary differential equation SIR model in a homogenous well-mixed population. We present the explicit equations of our model in an appendix. SIR models divide people into three categories: Susceptible, Infectious, and Recovered (SIR). We stick with this simplification, but we assume $M+1$ variants of the virus that can arise via escape mutations. For ease of exposition, we will often call these variants "drift levels" or sometimes simply "strains." We write $I(h)$, sometimes I_h, for those currently infected with drift level h. We reserve $h=0$ for the strain that initially infects the population. We do, however, explore introduction of other strains in the supplementary material. Upon recovery from a strain h infection, the individual moves from compartment $I(h)$ to compartment $R(h,0)$; the 0 in $R(h,0)$ indicates complete immunity to strain h. As this immunity wanes, this individual moves from $R(h,0)$ to $R(h,1)$, later to $R(h,2)$ and eventually to $R(h,P)$. We assume $P+1$ waning states for each drift level.

A key simplification in our model is that all drifting takes place at the time of transmission. Escape mutations arise during transmissions to individuals who already have some immunity from which the virus can escape. We do not follow the levels of virus mutation in the source and recipient individuals in a transmission, and we ignore how the transmission bottleneck might allow for multiple drifted viruses to be transmitted between hosts. The observations of (Lythgoe et al. 2021) that the transmission bottleneck is small and that the frequency of variation in the bottleneck is low indicate that this simplifying assumption is justified. We assume a common drifting scale between infectors and infectees. In other words, we put both the antigenicity of SARS-CoV-2 and the immune capacity of someone previously infected with the virus on the same scale. The infectee has the same position on the drifting scale as their last infection.

To model how escape mutations arise, we formulate two strain networks or patterns. The first of these relates to the strain in the source case in a transmission. This we denote as the pattern of *possible strain mutations*. The second is determined by the pattern of immunity in the host being reinfected. This pattern describes how immunity in a person being reinfected affects the realization of a possible strain mutation. Call this the *immunity driving and blocking pattern*. Immunity can drive mutation if one of the possible strain mutations in the source case escapes some of the immunity in the person being reinfected. Immunity blocks a possible strain mutation if the recipient of a transmission has more immunity to the drifted strain than they have to the strain in the source case that has not drifted.

To model possible strain mutations, we consider the collection of strains as the vertices or nodes of a network – the "possible strain mutation network" or simply the "strain network." An edge connects two strains in this network if one strain can mutate to the other. The "distance" between any two strains in this network is the minimal number of

network edges required to move from one strain to the other. Fig. 1 presents the three strain networks we considered. The top shape in Fig. 1 puts strains at the integer points on a line. This line has seven nodes, beginning with the node for the initial strain 0 on the left.

We examined this linear possible strain mutation network using two different immunity pattern driving and blocking patterns. The immunity blocking patterns are identical in all our models. That is because in all cases, drifting cannot increase the susceptibility of a virus to immunity in the host being infected. The immunity driving pattern differs between model 1 and models 2 or 3. Model 1 assumes that all immunity in the recipient individual that has been stimulated by any previous infection to one side of the source case strain can drive that source case strain to drift in the other direction to escape immunity in that individual. Models 2 and 3 assume that only immunity in the source case that was stimulated by a strain no more than one strain different from the source case strain can drive drifting.

To see if having extreme edges in the network influenced the interaction between waning and escape mutation drifting, we built model 3 by turning the line in model 2 into a circle, as pictured in Fig. 1. That involved changing the possible strain mutation network so that strain 6 can mutate just as easily back to strain 0 as to strain 5. Models 1-3 are symmetrical. For models 1 & 2, that means that model behavior is identical when the introduced strain is at either end. For model three it means the behavior is identical wherever infection is first introduced.

Models 1-3 represent variations on the SIR differential equation formulations where all mutations affect the same epitope. These variations could provide insights for formulating the effects of specific escape mutations examined molecularly.

In our fourth model, we envisioned immunity related to distinct epitopes. In the real world, there could be many distinct codons in an epitope where mutation would change the ability of previously stimulated immunity to prevent an infection. At each codon, changes to multiple amino acids are possible. We chose a simplification in which there were only three epitopes involved and only two codons relevant to only two amino acids for each epitope. These assumptions lead to the cube network in Fig. 1 with a connection between two nodes if they differed in the codons for one epitope.

We model the network of possible strain mutations by constructing an $(M+1)(M+1)(M+1)$ tensor that specifies which escape mutations can occur for a given strain network. The (h,j,h') entry in such a drift tensor is the probability that when an $I(h)$ infects an $R(j,k)$, strain h can mutate to strain h' in which case the new infectee enters compartment $I(h')$. For example, in model 1, if an infector in $I(1)$ infects a susceptible in $R(0,k)$, then according to the strain network in Fig. 1, strain 1 can only drift to strain 0 or strain 2. But the only possible drift is to strain 2 because of the residual immunity to strain 0 in the infectee. In the drift tensor,

$$\varphi(1,0,h') = \begin{cases} 1-D, & \text{if } h' = 1 \\ D, & \text{if } h' = 2 \\ 0, & \text{otherwise} \end{cases}$$

where D is the population drift rate. Similarly, an $I(2)$ who infects an $R(0,k)$ can only yield an $I(2)$ or with probability D an $I(3)$. The immunity
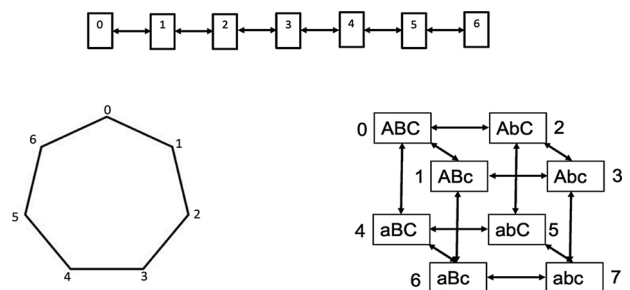

Fig. 1. The shapes of drifting patterns examined.

in the $R(0,k)$ will cause any virus that by chance drifted to level 1 to grow more slowly than the viruses that drifted to level 3 in that person. The exponential growth process would then effectively extinguish the level 1 virus in favor of the level 3 virus. For model 2,

$\varphi(h,j,h') = 0$ if $|h - j| > 1$.

For model 3,

$\varphi(h,j,h') = D$ only if $j = h \pm 1$ and $h - h' \neq h - j$, $(\mod (M + 1))$.

To illustrate the drift tensor in the 3-epitope model 4 in Fig. 1, suppose an I(aBc) also labeled as an $I(6)$ infects an R(ABC, k). By the strain network in Fig. 1, the aBc can only drift to ABc, aBC, or abc. However, residual immunity in codon B will impede drifts to ABc or to aBC; so the only possible immunity-escaping drift is to strain abc. We present drift tensors for all four models in Tables S1-S4 in the Supplementary Material.

Finally, we describe how we handle transmission in our model. We assume an effective contact rate B for transmission of the virus (contact rate times probability of infection per contact) when an infection in any I (h) meets a never-before infected susceptible in S. We modify this rate to $B \cdot Z(h,j,k)$ for encounters between infected individuals $I(h)$ and previously infected susceptible individuals in $R(j,k)$. The modified probability of transmission $B \cdot Z(h,j,k)$ increases as the distance $dist(h,j)$ between the two strains h and j increases and as the susceptible person's immune system wanes (higher k). In particular, we used

$$Z(h,j,k) = \left(\frac{k}{L} + \left(1 - \frac{k}{L} \right) \cdot \frac{\text{dist}(h,j)}{Q} \right) \tag{1}$$

where L is a constant $\geq P$ and Q is at least the maximum distance between strains in the drift network.

To initialize the epidemic, we introduced one infection per 1 million into a continuous population nominally scaled to present results per 1000 individuals. All time scales were set to a week. We assume an average of 2 weeks from onset of infection to full recovery. We set B = 1, implying a basic reproduction number $R_0 = 2$. We worked with 7 drift levels in models 1, 2, and 3. In model 4, we assumed there were 3 independent dichotomous alleles, so that there were $2^3 = 8$ drift levels. Table S5 in the SM provides some intuition for the effects of varying W. For example, in model 1, at waning rate $W = 0.1$, it takes 57 weeks for half of those entering $R(0,0)$ to reach $R(0,6)$. For $W = 0.01$, that process takes 11 years.

Our waning functions have no redundant immunity. This means that as soon as there is any waning, there is susceptibility. The six waning steps are of equal size. In the last waning state, the susceptibility of previously infected individuals is 6/7ths of a fully susceptible, never infected individual. Drifting is likewise divided into six drifting steps and 7 drift levels for models 1 and 2. For models 3 and 4, however, there are only 3 steps to the most distant drift state, so we double the size of immunity loss for each step while leaving the last state having 6/7ths of full susceptibility. We took $Q = 7$ in models 1 and 2, and $Q = 3.5$ in models 3 and 4.

Further understanding of the model structure can be gained in two ways. The first is reading the mathematical description of the model in the appendix. The second is to read the annotation of the code. The code is structured so that the influences on each variable change are made explicit. A list of parameters, their definitions, and values is in the appendix.

3. Results: Model behaviors observed across the four models: without vaccination

In the absence of vaccination, the behavior of the four different models was remarkably similar. In particular, without waning there was no drifting no matter how high the drifting parameter was set. In the absence of waning, it took 78 years of new susceptible births before a second epidemic appeared. With tiny amounts of waning but no drifting

$(W = 0.000001, D = 0)$, results were similar. (See Figs. S1 and S2 in SM.) But with just an equally tiny amount of drifting $(W=D = 0.000001)$, the first rebound epidemic followed just a few years after the first. See the bottom right panel of Figs. 2–5. So, at low levels of waning, the joint effects of waning and drifting are far greater than multiplicative. That is because drifting adds to the susceptibility of the population. While waning affects only those experiencing the waning, drifting status is transmitted and affects many others.

A notable outcome across all four models is the identical pattern of the first epidemic wave across all waning and drifting patterns. The assumptions of population homogeneity with random contacts and no behavior change lie behind these identical patterns. But the key element is that drifting only occurs with reinfections. There are some minor imperceptible differences at the highest waning and drifting rates as some reinfections begin appearing late in the first epidemic, especially in model 4.

Only at the highest waning rates given the lowest drifting rates (bottom left in the 4 figures) do we see a rebound epidemic after the first epidemic where the rebound epidemic has the same strain as the first epidemic. For $W = 0.1$ there is no prolonged interval of low infection rates between the first epidemic peak and the second.

For waning levels W of 0.01 or lower (columns 2,3,4), all four models show distinct epidemics where the second epidemic has different strains from the first. These epidemics are separated by a period of low incidence after the first epidemic. The lowest incidence period occurs between the first epidemic and the first rebound epidemic. For $W = 0.01$ and $D = 0.0001$, the prevalence of infection is low enough for stochastic die out to be likely in all models except for model 4. But the levels are not extremely low in any case. A more detailed presentation of this is found in the supplementary material.

There are some ways that models 2 and 3 differ from models 1 and 4. At waning rates of 0.01 or lower, models 1 and 4 have only sequential epidemics with the second epidemic wave dominated the strain most distant from the first. Models 2 and 3 have less predictable strain occurrences and less predictable epidemic patterns.

The four models have different intensities of new escape mutations. They are ordered as models 4, 1, 3, and 2 in this regard. There is no simple scaling of model parameters that can make the patterns between any two pairs of models identical. Model 4 has the most drifting because it has many different paths of three short steps to almost complete loss of immunity. The large difference between model 1 and 2 is explained by the fact that for model 2 only a small fraction of encounters with previously infected persons that drive drifting in model 1 continue to do so in model 2. The higher rates of drifting in model 3 compared to model 2 (which both have drifting driven only by the nearest strain difference) is partly explained by each strain in model 2 having two strains that are maximally different. Recall from expression (1) that maximally distant strains have the lowest cross-immunity to each other. A further explanation is that each escape mutation makes a larger reduction in immunity in model 3 since it takes only 3 steps to get maximally different in model 3 but 6 in model 2. A difference between model 2 and the others is that at waning rates of 0.01 or less the first rebound epidemic does not have the most distant strain from the original epidemic.

Further comparisons of the different models across some of the higher parameter values with comparisons across all four models in the same graph are presented in the Supplemental Material.

3.1. Equilibrium infection levels

Prevalence reaches an equilibrium in all four models, for all parameter values. At that equilibrium in the four models we examined, all strains mixed evenly with all other strains. Endemic equilibrium infection levels are an increasing function of the waning rate W and are mostly unaffected by the drifting parameter D. The drifting parameters accelerate the attainment of equilibrium, but for the most part they do not change equilibrium levels. As seen in Fig. 6, the equilibrium
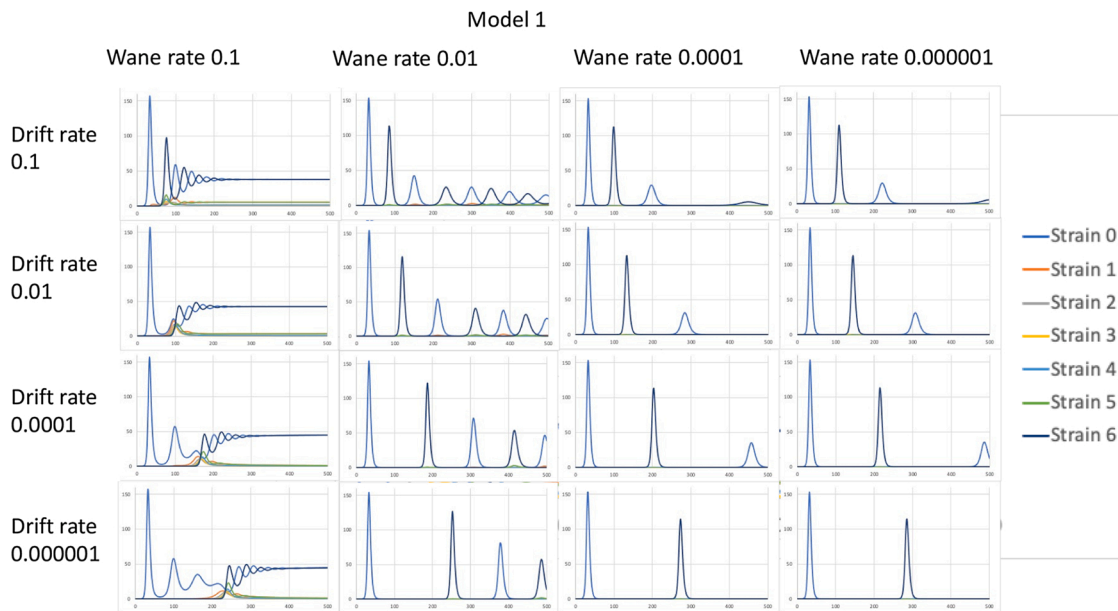
Fig. 2. Effects of large changes in the waning and drifting parameters on infection patterns during the first 500 weeks for model 1 specifying strain series. The values on the *x*-axis are weeks from 0 to 500; the values on the *y*-axis are number of those infected at time *x*.
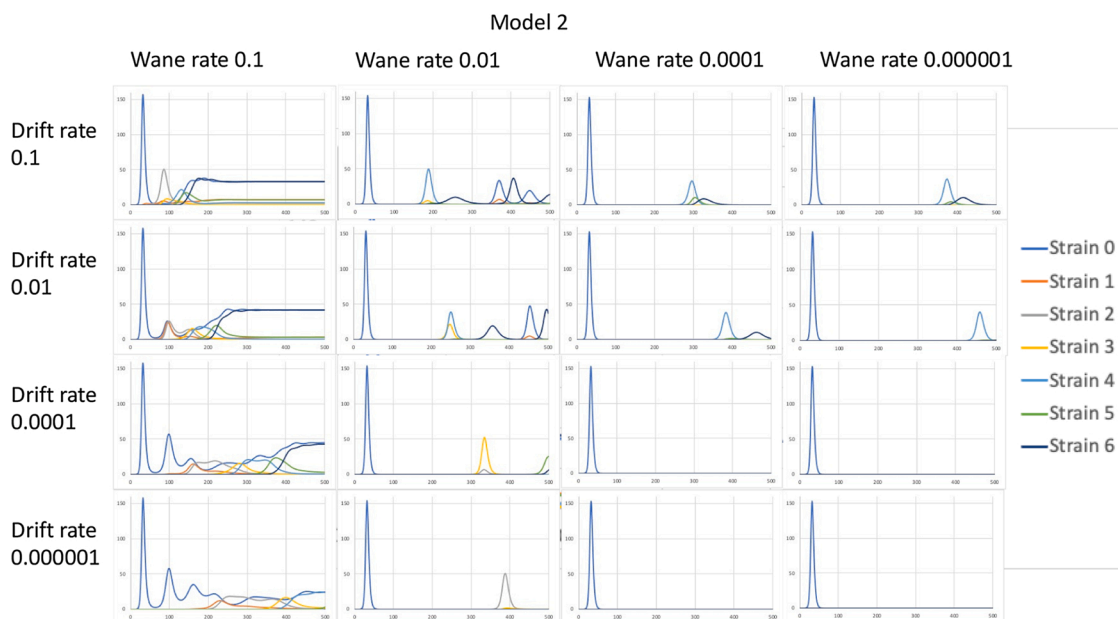

Fig. 3. Effects of large changes in the waning and drifting parameters on the number infection (*y*-axis) during the first 500 weeks (*x*-axis) for model 2, specifying strain series. Axes are identical to model 1.

infection levels were identical for models 1 and 2 and nearly identical to these values for model 4. But they were considerably higher for model 3; in model 3 each drift level has two different drift levels that are maximally different from it. For all the other models, each drift level has only one. Overall, the endemic reinfection levels at the higher waning parameter values are in the ranges observed by (Petrie et al. 2021).

4. Model behaviors observed across the four models: with vaccination

Vaccination effects were explored by beginning vaccination at the end of the first epidemic and keeping it constant thereafter. Vaccination rates of 0.25 and 1.0 per person per year were examined. The vaccine in

our model generated the same immunity as an infection. The immunity is against infection; there is no immunity against disease given infection in this model. Specifically, vaccination moves a susceptible to state *R* (0,0), where drift level 0 is the initial infecting level – the one that thoroughly dominates the epidemic wave that precedes the introduction of the vaccine. The models discussed here have a small number of epitopes and no redundant immunity. That makes the insights generated by our analysis relevant for constructing more realistically detailed models, but less relevant for interpreting real world vaccine patterns.

When both the waning rate and drifting rate are at 0.1 as in Fig. 7, we see for all models that vaccination has small but beneficial effects on the first rebound epidemic for models 1 and 4 with larger effects for models 2 and 3. The effects on endemic levels are more uniform across models;
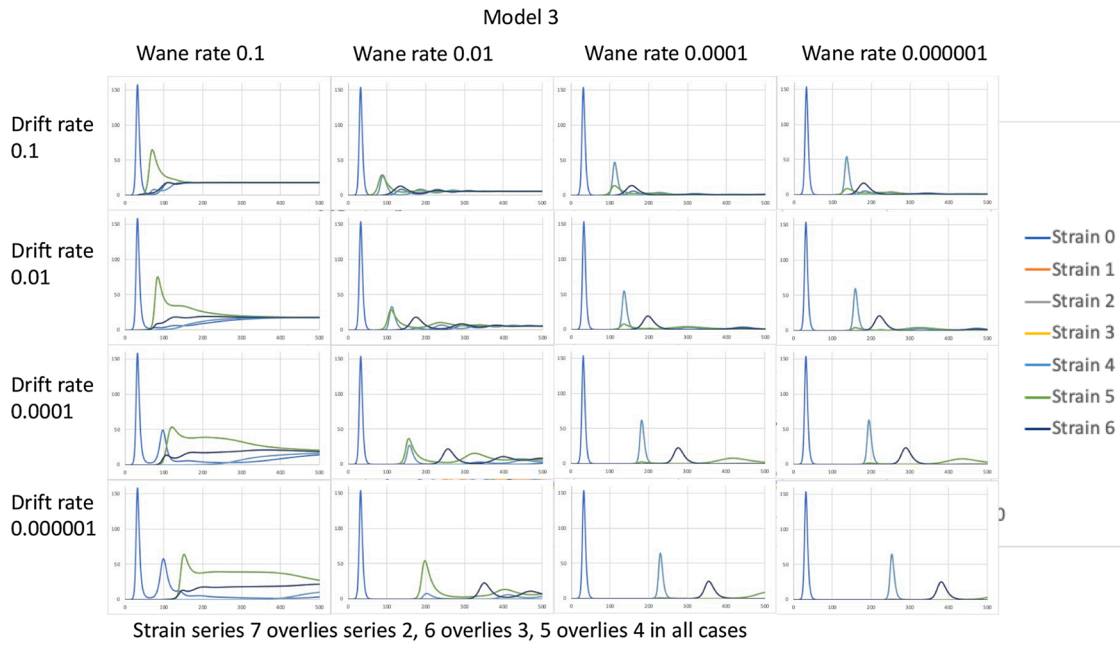
Fig. 4. Effects of large changes in the waning and drifting parameters on the number infection (*y*-axis) during the first 500 weeks (*x*-axis) for model 3, specifying strain series. Axes are identical to model 1.

Fig. 5. Effects of large changes in the waning and drifting parameters on the number infection (*y*-axis) during the first 500 weeks (*x*-axis) for model 4, specifying strain series. Axes are identical to model 1.
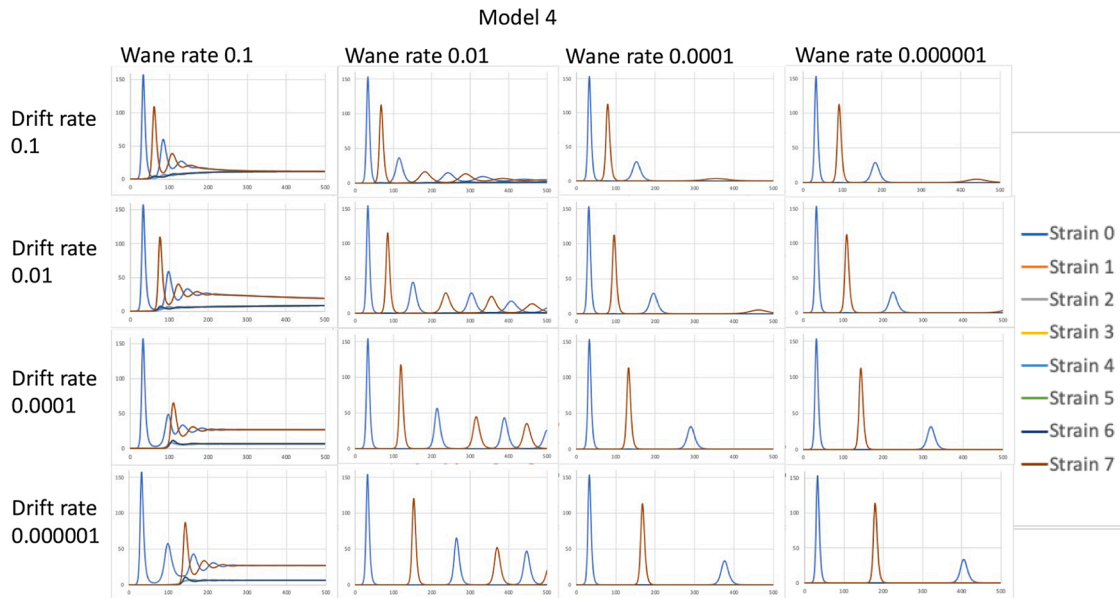
vaccination decreases infection prevalence at equilibrium.

When the waning rate is decreased to 0.01 as in Fig. 8, however, we see small but positive vaccine effects when the vaccination rate is only about a quarter of the population per year. However, when the vaccination rate goes up to 1 per year, vaccination has negative effects. It increases the frequency of rebound epidemics and raises the equilibrium levels of infection.

Similar patterns are seen in Figs. S6 and S7 where the drifting level is lowered to 0.01. At waning rate 0.1 vaccines reduce infection levels a little at both vaccination rates. At waning rate 0.01 the low vaccination rate slightly lowers endemic infection levels. At the high vaccination rates, endemic infection levels are higher than without vaccination.

These effects of high vaccination rates raising endemic infection

levels occur in all cases because high levels of vaccination eliminate strains with drift levels like those of the original pandemic strain and the vaccine. This leads to more rapid evolution away from the original strain and results in an increase in the frequency of individuals that have the highest levels of susceptibility to the original drift level to which the vaccine was constructed. For example, in the first column of Fig. 8 – Model 1 with *W = 0.01,* when there is no vaccination, extreme strains 0 and 6 alternate domination of subsequent epidemic waves. Full vaccination strengthens the population's immunity to strain 0 so that in this case all epidemic waves after the first are dominated by strain 6. In this scenario, a recently recovered individual – in some *R(j,k)* – is more likely to encounter an infector in *I(6)* than they would in the no-vaccination situation. As seen in the susceptibility function (1), these *I*
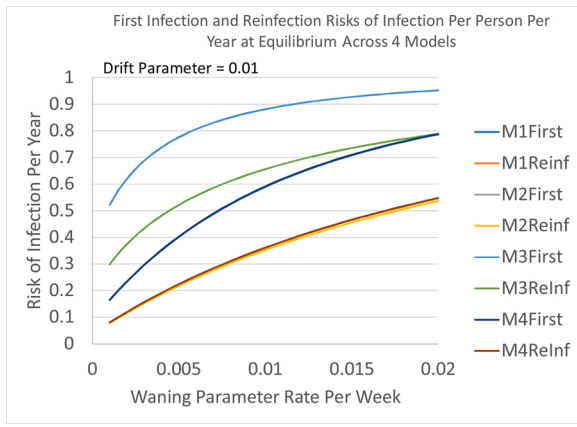
Fig. 6. Graphs of the risk of first infection and risk of reinfection at equilibrium for all 4 models as the waning rate W increases. The top two graphs are for model 3, the bottom two are for models 1, 2, and 4. In each case, the risk of first infection is greater than the risk of reinfection. M4First overlays M1First and M2First. M2Reinf overlays M1Reinf.

(6) encounters lead to higher total population susceptibility than would be encountered with a wider distribution of strains. Vaccination in Model 4 has similar effects for $W = 0.01$. Without vaccination, strains 0 (ABC) and 7 (abc) dominate alternate epidemic waves. With full vaccination, strain 7 dominates every wave after the first, leading to higher population susceptibility.

Model 3 is less subject to these effects for the same reasons it stood out regarding parameter effects when there was no vaccination. In model 3, the number of escaped strains that can take advantage of immunity levels stimulated by the vaccine or pandemic strain is greater so the vaccine has fewer individuals it can drive into the most drifted state.

Figs. S8 and S9 make it easier to see the differences in vaccine effects when the waning rate changes from 0.01 to 0.1 by putting all three vaccination rates in the same figure.

The effects of other parameter changes such as the transmission parameter, the place in the drifting matrices that pandemic transmission begins, and how much immunity loss occurs during drifting are

discussed in supplementary material section 6.

5. Generation of cross-neutralization assay and epitope specific serology results

Cross neutralization assays have long been used to determine whether new strains of viruses have developed escape mutations. But these assays have not previously been used to fit waning and drifting parameters of population models.

A strength of our model formulation is that it generates population patterns of immunity. As a result, our model can be fit to population level serology data and thus inform decisions about which epitope conformations to include in updated vaccines. Describing how cross neutralization tables are generated by the model and how they change over time given different parameter values illustrates the potential of fitted models to be used in vaccine composition decisions.

At a population level, cross-neutralization analyses are performed on a sample of individuals from a population. These indicate the strains to which a population is most susceptible. Each individual's sample is assayed separately against each strain. The procedure in the lab is to divide each sample of sera into 10 titers by dilution. Titer 1 is undiluted; titer 2 is diluted 1-1; titer 3 is titer 2 diluted 1-1, and so on. Each of these titers is mixed with a sample of the first virus. For each individual, the highest numbered (weakest) titer that neutralizes the virus is recorded. These same serum samples are also mixed with the second virus and the highest numbered neutralizing titer is also recorded for each individual. The joint distribution of the two is then analyzed.

SARS-CoV-2 neutralization titers differ markedly across individuals. That is true even when everyone is assayed at the same time after infection or vaccination (Dan et al. 2021). Waning across different times since last infection adds to the variation between individuals. But the variation between individuals is balanced out statistically. If there is a statistically significant difference in the mean titers for two different viruses, then the viruses have drifted to provide an escape mutation. If the times when different viruses circulated in the population sampled is known, both waning and drifting can be assessed.

To generate cross neutralization data from our models' output, we use the $Z(h,j,k)$ function as formulated by equation (1) to calculate the
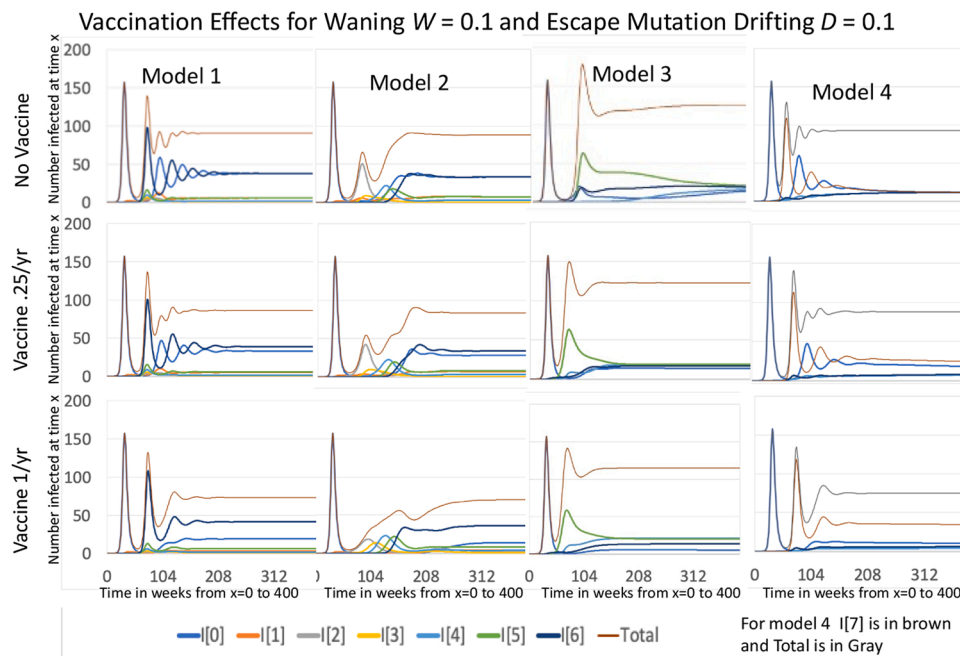

Fig. 7. For each of the 4 models, W and D are fixed 0.1. The first row presents the graphs for the case of no vaccination; the second row presents partial vaccination (25% of the population per year); the third row presents full vaccination per year.
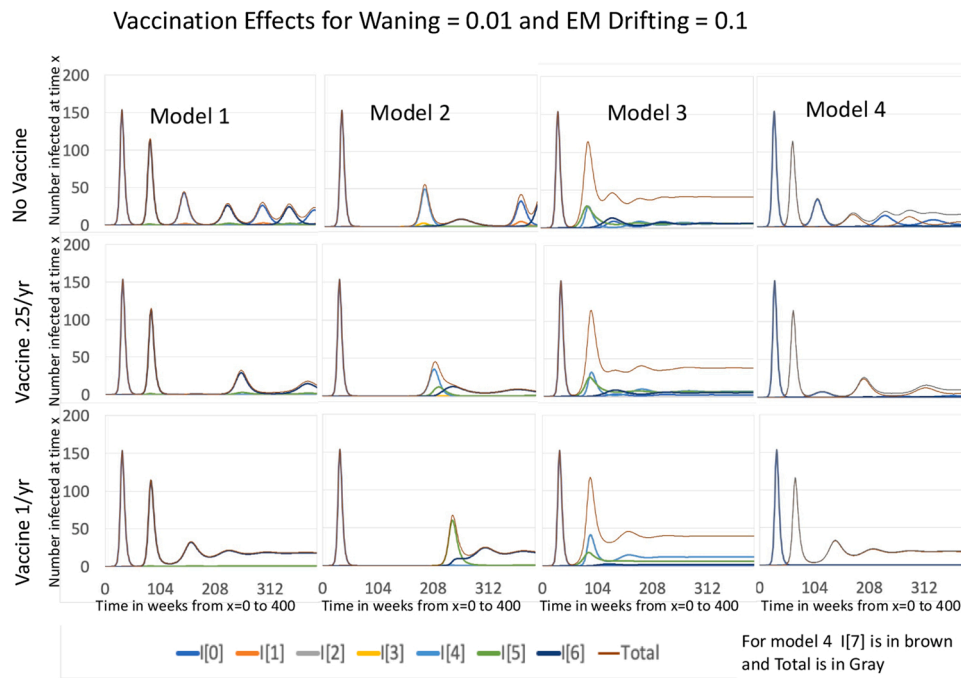
Fig. 8. This is the analog of Fig. 7, but with the waning rate *W* at 0.01 instead of 0.1. Full vaccination is more problematic here than in Fig. 7.

susceptibility of all individuals (or more correctly population segments since we model continuous populations rather than individuals) who have recovered from a previous infection. Since the *Z* function is a transmission parameter, it corresponds to the inverse of the neutralizing level. To make that number correspond to a titer, we divide the interval [0,1] into 10 equal subintervals: $Y_1, \ldots, Y_{10}$, where $Y_1 = [0,.1]$. At time T and within drift level h_1, we assign to each susceptible individual a "titer number for time T and drift level h_1" as follows. For an individual in $R(j, k)$ at time T, assign as "titer number" the number m for which subinterval Y_m contains $Z(h_1,j,k)$, as in expression (1). Assign number 1 to those in *S*. Similarly, construct for each susceptible a titer number for time T and drift level h_2. Form a 10×10 matrix whose (i,j)th entry is the number of population who had titer number i for strain h_1 and titer number *j* for strain h_2 at time T. This matrix is the basis of our cross-neutralization analysis. We present an example of such a construction in the Supplementary Material.

Comparison of model-generated cross-neutralization tables and corresponding tables from serology labs can be used to fit the model waning and drifting parameters. Such model fits can then be used to project how the immunity levels in the population will affect the spread of new virus variants with escape mutations. They can also be used to project how quickly further escape mutations might emerge. The validity of such projections requires more models that specify a series of specific potential escape mutations. The type of data generated by (Shrock et al. 2020) in combination with the type of data generated by (Greaney et al. 2021) could be helpful in this regard.

There are many epitopes and a wide a variety of immune responses to those epitopes. Thus, a model to capture all that information extensively enough to validate a vaccine decision will be complex. Consequently, deciding how to best validate a vaccine decision is a crucial issue.

6. Using the model and data to make decisions about vaccine composition

The model we have presented is a first step to make decisions about vaccine composition. Next steps involve further model elaboration and analysis as well as fitting the model to data. Two types of data would be useful: 1) the rate of fixation of mutations at a population level, and 2) acquired population immunity data. For the first, key parameters to fit

involve increased transmissibility and immune escape. To estimate those parameters, the specific epitopes and the specific mutations of those epitopes that have been observed need to be specified in the model structure. For example, the prominent transmission enhancing or immunity escaping mutations described in (Harvey et al. 2021) could be individually specified in the model. Then prior probabilities for the transmission and immune escaping parameters could be established using laboratory based deep mutational scanning for attachment to the ACE2 receptor or the attachment of epitope specific antibodies to the observed mutations as done by (Greaney et al. 2021). Finally, the model could be fit by ABC-SMC to patterns of infection in the population to different strains. Even better data may be coming soon from single cell sequencing of FACS selected immune cells that determine the epitopes to which SARS-CoV-2 immune responses have been developed.

The presence of strains with escape mutations is only one factor affecting the choice of mutations to include in vaccines. Another is the immunity levels in the population against different mutations. These determine which strains, and which specific escape mutations, will circulate. It would not be optimal to include a mutation in a vaccine if the targeted mutation is expected to have low levels of circulation in the absence of the vaccine. Data on who has immunity directed to specific mutation states involving original or altered amino acids would serve to better estimate many model parameters.

6.1. Integrating models and data to improve decisions

There is no way to validate one model for informing all decisions. A process is needed that accommodates the model to available data and identifies the most informative data that is lacking. Focusing on two sources of model-based decision errors can bring the data and models into a favorable balance for making decisions. These are:

1 A simplifying assumption, if realistically relaxed, would change the decision
2 An unrecognized alternative model parameter set that fits the data would change the decision

Practical identifiability analyses are key to addressing these two sources of error. The first step is to identify the parameter space of the

model that leads to a decision. The decision could be multifaceted with different parts of parameter space favoring different vaccine modifications and some parts favoring no change to the vaccine. To simplify our description, in Fig. 9 we make the space binary with the grey area favoring modification A and the yellow area favoring modification B. In a second step, the model space that is consistent with the data is demarcated. Three possible demarcations are illustrated. Identifiable decisions could favor either A or B or have part of their space consistent with A and a different part be consistent with B. In this latter case the decision is not identifiable.

Subsequent steps are different depending upon whether the decision is identifiable or not. If it is, then the robustness of the decision should be assessed by realistically relaxing assumptions in the model to see if that changes a decision should be pursued. In general, that will decrease identifiability. When the decision is not identifiable, then new data or better use of the existing data should be sought. If the decision is just to accept a scientific theory, then this process should go on forever. But if there is a deadline to make a vaccine for a coming season, then professional judgement is needed. We believe that better decisions will be made when that judgement is focused on potential robustness of decisions to realistic relaxation of simplifying assumptions and on identifiability of decisions rather than on the weight of evidence for one decision or the other just using the current model.

We believe that epitope specific models and data can feasibly be developed. More thoughts on that issue are presented in the supplemental material.

7. Discussion

The main reason for changing SARS-CoV-2 vaccine composition in the future is the emergence of escape mutations. The emergence of new SARS-CoV-2 immune escape mutations in our model is like that seen in the real world. Escape mutations did not appear until there were opportunities for reinfections. Transmission enhancing mutations like D614 G, on the other hand, were almost immediate. This speaks to the importance of modeling escape mutations as occurring upon reinfection. Models of that process describe how waning and escape mutations interact. We have laid out an ODE model structure for such an interaction.

Building on the foundational work establishing the discipline of phylodynamics (Grenfell et al. 2004), the potential effects of SARS-CoV-2 escape mutations have been abstractly imputed by Saad-Roy and colleagues (Saad-Roy et al. 2021; Saad-Roy et al. 2020). The model we present here, extends the theoretical foundations for such an analysis and enables direct computation of effects.

We are extending the theoretical foundations of our model in several ways. An individual based stochastic formulation elaborates the transmission process with virus excretion rates, environmental survival, up take rates, and dose response formulations. It also allows for including
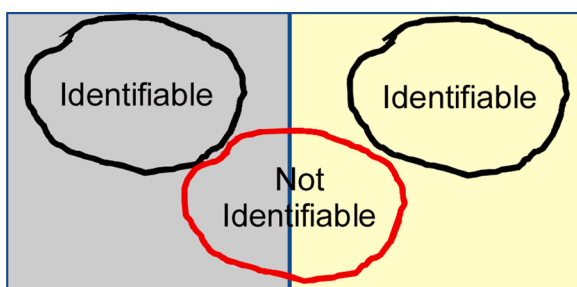
many more distinct episodes and can be formulated to integrate mutations in the same epitope as well as large numbers of epitopes. In both ODE and individual based models, the natural history of immunity has been elaborated so that reinfection does not eliminate previously acquired immunity as the model presented here does. These new models will facilitate exploring the implications of diverse patterns of waning and escape mutation drifting within and between epitopes.

Perhaps the number of possible escape mutations with little cost to transmissibility is limited. That would be consistent with the laboratory-based induction of mutations by (Greaney et al. 2021) where most mutations that escaped the effects of monoclonal antibodies or convalescent sera also decreased binding to the ACE2 receptor. In that case, future escape mutations could increasingly be associated with lower transmissibility.

As the number of escape mutations increases and their co-occurrence with mutations that decrease transmission increases, the task of making good vaccine composition choices for future vaccines will become more complicated. One complicating factor is that the low rate of SARS-CoV-2 escape mutations means that different mutations will emerge in different parts of the world. When travel brings those mutations together, their interaction effects will have to be predicted. We have laid out a path for addressing such complications that includes both realistic relaxation of simplifying assumptions and searches for data that make decisions more identifiable.

However, the differences we have observed between simple models with few potential mutations indicate great potential complexity in the generation of multiple mutations. As we build models with more potential mutations that differ not only in their drift matrices but also in how they affect transmissibility and how immune responses to them generate joint effects with other mutations (Koopman 1985) this complexity will grow. But the potential for unique and highly effective vaccine constructs might also grow.

Author statement

All authors have read and approved the final version. James Koopman and Carl Simon jointly conceived the issues to be addressed, wrote the software, analyzed the models, produced the figures, and wrote the paper. Richard Salter contributed ideas for approaching the software. Wayne Getz helped develop approaches to the mathematics.

Declaration of Competing Interest

Koopman and Simon have no conflict of interest

Getz and Salter are developers of Numerus software which they are developing for sale. The work presented in this paper was not done with this software. But this software will facilitate certain steps in the Decision Robustness and Identifiability Analysis strategy that is presented in the paper. In particular, it will facilitate integrating the complex processes in the model presented into other models. It will also facilitate the transition from ODE models to discreet individual stochastic process models.

Fig. 9. Defining decision identifiability: The grey area is consistent with one decision, the yellow area with another. Possible areas consistent with data are illustrated for two data sets where the parameter sets show identifiable parameter sets and one where the parameter sets do not lead to an identifiable decisions.

Appendix A. Mathematical formulation details

In this Appendix, we present the SIR differential equation system of our SARS-CoVid-2 models 1&2. Recall from our discussion in the main text that the compartments in our model are:

- S, never infected susceptibles,
- $I(h)$ or I_h, those infected with strain h, $h = 0, 1,...,M,$
- $R(j,k)$, previously infected susceptibles whose last infection was strain j and whose level of immunity to strain j is k, for $k = 0,1, ..., P.$

So, there are $M + 1$ strains with strain 0 being the original strain and $P + 1$ levels of immunity, with level 0 that of full immunity.

The effective contact rate – roughly the probability of transmission – between a susceptible in S and an infective in $I(h)$ is B. Three important processes in the dynamic are the strain network, the drift tensor $\varphi(h,j,h')$, and the transmissibility function $Z(h,j,k)$. The strain network is a network whose nodes are the strains in the system with two strains connected by an edge if one can mutate to the other. The expression $\varphi(h,j,h')$ gives the probability that when an individual in $R(j,k)$ is infected by an individual in $I(h)$, strain h will drift to strain h'. The transmissibility function $Z(j,h,k)$ when multiplied by B gives the effective contact rate for an encounter between a possible infector in $I(j)$ and a susceptible in $R(h,k)$:

$$B \bullet Z(j, h, k) = B\left[\left(\frac{k}{Q}\right) + \left(1 - \frac{k}{Q}\right)\left(\frac{\text{dist}(h,j)}{L}\right) \right] \quad (1)$$

This formulates independent joint effects of waning and drifting on infection risk with drifting adding susceptibility beyond the current level of waning. It implies that drifting and waning operate on the same scale in terms of ability to increase susceptibility.

Note that $\underline{Z}$ increases with the level of waning k in the susceptible and the distance between the strains j and h in the strain network.

Vaccination occurs at the end of the first epidemic wave when strain 0 still dominates. A vaccinated susceptible moves to compartment $R(0,0)$ with temporary complete immunity to strain 0. The default vaccination rate is $v = 0.02$/week, which is more than one person per year. We also consider a weaker vaccination program with $v = 0.005$/week.

$$\frac{dS}{dt} = mN - mS - BS \sum_{j=0}^{M} \frac{I_j}{N} - vS$$

$$\frac{dI_h}{dt} = \frac{B}{N}\left(I_h S + \sum_{j=0}^{M} \sum_{i=0}^{M} \sum_{k=0}^{P} Z(i,j,k) \cdot \phi(i,j,h) I_i R_{jk} \right) - (g+m)I_h, \; h = 0,\ldots,M$$

$$\frac{dR_{jk}}{dt} = gI_j \delta_{\{0\}}(k) - \frac{B}{N}\left(\sum_{h=0}^{M} Z(h,j,k)I_h \right) R_{jk} - mR_{jk} - W_k R_{hk}\delta_{\{0,\ldots,P-1\}}(k) + W_{k-1} R_{h,k-1}\delta_{\{1,\ldots,P\}}(k)$$

$$- vR_{jk} + v\delta_{\{(0,0)\}}(j,k)\left(S + \sum_{p=0}^{P} \sum_{i=0}^{M} R_{ip} \right), \; j = 0,\ldots,M; \; k = 0,\ldots,P.$$

Here, for any subset Y of a set X, $\delta_Y(x) = \begin{cases} 1, \text{if } x \in Y \\ 0, \text{if } x \notin Y. \end{cases}$

So, $\delta_{\{0\}}(k) = \begin{cases} 1, \text{if } k = 0 \\ 0, \text{otherwise} \end{cases}$; $\delta_{\{0,\ldots,P-1\}}(k) = \begin{cases} 1, \text{if } k = 0,\ldots,P-1 \\ 0, \text{otherwise, i.e., } k = P. \end{cases}$

$\delta_{\{(0,0)\}}(j,k) = \begin{cases} 1, \text{if } j = k = 0 \\ 0, \text{otherwise.} \end{cases}$

The first equation describes the infection and vaccination of never infected susceptible individuals. The second set of equations describes the dynamics of those infected with drift level h – the I_h's, who recover at rate g and die at rate m. New I_h's rise when an I_h infects an S, infects any R_{jk} without drifting, or when an I_i drifts to an I_h upon infecting an R_{jk}. The probability of the latter occurrence is the probability $Z(i,j,k)$ that any given I_i will infect an R_{jk} times the probability $\phi(i,j,h)$ from the drift tensor that the I_i will drift to an I_h upon such an infection. Models 1 and 2 differ only with regard to this drift tensor.

In the third set of equations, R_{jk}'s increase when an I_j recovers or when an $R_{j,k-1}$ wanes. R_{jk}'s decrease when they wane to an $R_{j,k+1}$ or upon vaccination. The last line in the above equations keeps track of the vaccination process when the newly vaccinated enter R_{00}.

We simulated the model using the Berkeley Madonna Software (Madonna 2021) always checking to see that the shortening the step size did not change the results. For the simulations in this report we set effective weekly transmission rate parameter $B = 1$ or 1.5 and weekly rate of recovery $g = 0.5$, so that the underlying basic reproduction number is $R_0 = 2$ or 3. The birth and death rates were set at $1/(75 \times 52)$. All time scales were set to a week. We introduced one infection per 10 million into a continuous population denoted as having size 1000. Numerical solution of the model used Runge-Kutta 4 and the stability of numerical solutions were evaluated across smaller time steps.

Symbol Summary

S Never infected susceptibles

$I(h), I_h$ Those currently infected with strain h, $h = 0$ initial strain

$R(j,k), R_{jk}$ Formerly infected susceptibles, whose previous infection was strain j and whose level of immunity to strain j is k

$M + 1$ Number of drift levels ("strains"). Initial strain = strain 0.

$P + 1$ Number of immunity (waning) levels; Level 0 is full immunity

m weekly rate of birth (into S) and of background death

u value of m in the Madonna runs

B effective contact rate for contacts between those in S and those in any I(h)

N Total population, $N = S + \sum I(h) + \sum R(j,k)$

v Vaccination rate per week

$Z(i,j,k)$ Transmissibility function (1). Multiplier of B for contact between Infected in $I(h)$ and susceptible in $R(j,k)$

Q Denominator in *Z* for waning level: $Q \geq P$

L Denominator in *Z* for drift level: $L \geq$ max distance between any 2 strains

$\varphi(i,j,h)$ Probability that when an infected in *I(i)* infects a susceptible in *R(j,k)* the newly infected will be in *I(h)*; the infecting strain will drift from *I* to *h*.

D probability that a drift away from infecting strain *i* occurs at all.

W_k weekly rate of waning from waning level *k* to level *k+1*.

g Rate of recovering from infection: *I(h) –> R(h,0)*.

T Time in weeks

Symbol values in Madonna runs:

S: Initial S(0) = 999.9999

I(h): Initial values I(0) = 0.0001 at time 0, all other I(h) = 0 at time 0.

R(j,k): all initial values = 0.

N = 1,000 for all *t*.

g = 0.5

B = 1 (= 1.5 in some SM runs)

V = 0, 0.005, 0.02 for no vaccination, partial vaccination, full vaccination, respectively.

$W_k=W$, constant for all waning levels *k*. Values varied from 0.1 to 0.000001

D takes on varying values from 0.1 to 0.000001

u or *m*: 1/(75 × 52)

Appendix B. Supplementary data

Supplementary material related to this article can be found, in the online version, at doi:https://doi.org/10.1016/j.epidem.2021.100484.

References

Andreasen, V., 2003. Dynamics of annual influenza A epidemics with immuno-selection. J Math Biol 46, 504–536.

Dan, J.M., Mateus, J., Kato, Y., Hastie, K.M., Yu, E.D., Faliti, C.E., Grifoni, A., Ramirez, S. I., Haupt, S., Frazier, A., Nakao, C., Rayaprolu, V., Rawlings, S.A., Peters, B., Krammer, F., Simon, V., Saphire, E.O., Smith, D.M., Weiskopf, D., Sette, A., Crotty, S., 2021. Immunological memory to SARS-CoV-2 assessed for up to 8 months after infection. Science 371.

Greaney, A.J., Starr, T.N., Gilchuk, P., Zost, S.J., Binshtein, E., Loes, A.N., Hilton, S.K., Huddleston, J., Eguia, R., Crawford, K.H.D., Dingens, A.S., Nargi, R.S., Sutton, R.E., Suryadevara, N., Rothlauf, P.W., Liu, Z., Whelan, S.P.J., Carnahan, R.H., Crowe Jr., J.E., Bloom, J.D., 2021. Complete Mapping of Mutations to the SARS-CoV-2 Spike Receptor-Binding Domain that Escape Antibody Recognition. Cell Host Microbe 29, 44–57 e9.

Grenfell, B.T., Pybus, O.G., Gog, J.R., Wood, J.L., Daly, J.M., Mumford, J.A., Holmes, E. C., 2004. Unifying the epidemiological and evolutionary dynamics of pathogens. Science 303, 327–332.

Harvey, W.T., Carabelli, A.M., Jackson, B., Gupta, R.K., Thomson, E.C., Harrison, E.M., Ludden, C., Reeve, R., Rambaut, A., Covid- Genomics UK Consortium, Peacock, S.J., Robertson, D.L., 2021. SARS-CoV-2 variants, spike mutations and immune escape. Nat Rev Microbiol.

Huddleston, J., Barnes, J.R., Rowe, T., Xu, X., Kondor, R., Wentworth, D.E., Whittaker, L., Ermetal, B., Daniels, R.S., McCauley, J.W., Fujisaki, S., Nakamura, K., Kishida, N., Watanabe, S., Hasegawa, H., Barr, I., Subbarao, K., Barrat-Charlaix, P., Neher, R.A., Bedford, T., 2020. Integrating genotypes and phenotypes improves long-term forecasts of seasonal influenza A/H3N2 evolution. Elife 9.

Kissler, S.M., Tedijanto, C., Goldstein, E., Grad, Y.H., Lipsitch, M., 2020. Projecting the transmission dynamics of SARS-CoV-2 through the postpandemic period. Science 368, 860–868.

Koopman, J.S., 1985. Analyzing the joint effects of two antibodies and the design of molecularly engineered vaccines. J Theor Biol 116, 569–585.

Lavine, J.S., Bjornstad, O.N., Antia, R., 2021. Immunological characteristics govern the transition of COVID-19 to endemicity. Science 371, 741–745.

Lythgoe, K.A., Hall, M., Ferretti, L., de Cesare, M., MacIntyre-Cockett, G., Trebes, A., Andersson, M., Otecko, N., Wise, E.L., Moore, N., Lynch, J., Kidd, S., Cortes, N., Mori, M., Williams, R., Vernet, G., Justice, A., Green, A., Nicholls, S.M., Ansari, M.A., Abeler-Dorner, L., Moore, C.E., Peto, T.E.A., Eyre, D.W., Shaw, R., Simmonds, P., Buck, D., Todd, J.A., Group Oxford Virus Sequencing Analysis, Connor, T.R., Ashraf, S., da Silva Filipe, A., Shepherd, J., Thomson, E.C., Covid- Genomics UK Consortium, Bonsall, D., Fraser, C., Golubchik, T., 2021. SARS-CoV-2 within-host diversity and transmission. Science 372.

Madonna, Berkeley. 2021. https://berkeley-madonna.myshopify.com/.

Petrie, J.G., Bazzi, L.A., McDermott, A.B., Follmann, D., Esposito, D., Hatcher, C., Mateja, A., Narpala, S.R., O'Connell, S.E., Martin, E.T., Monto, A.S., 2021. Coronavirus Occurrence in the HIVE Cohort of Michigan Households: Reinfection frequency and serologic responses to seasonal and SARS coronaviruses. J Infect Dis.

Saad-Roy, C.M., Morris, S.E., Metcalf, C.J.E., Mina, M.J., Baker, R.E., Farrar, J., Holmes, E.C., Pybus, O.G., Graham, A.L., Levin, S.A., Grenfell, B.T., Wagner, C.E., 2021. Epidemiological and evolutionary considerations of SARS-CoV-2 vaccine dosing regimes. Science 372, 363–370.

Saad-Roy, C.M., Wagner, C.E., Baker, R.E., Morris, S.E., Farrar, J., Graham, A.L., Levin, S. A., Mina, M.J., Metcalf, C.J.E., Grenfell, B.T., 2020. Immune life history, vaccination, and the dynamics of SARS-CoV-2 over the next 5 years. Science 370, 811–818.

Shrock, E., Fujimura, E., Kula, T., Timms, R.T., Lee, I.H., Leng, Y., Robinson, M.L., Sie, B. M., Li, M.Z., Chen, Y., Logue, J., Zuiani, A., McCulloch, D., Lelis, F.J.N., Henson, S., Monaco, D.R., Travers, M., Habibi, S., Clarke, W.A., Caturegli, P., Laeyendecker, O., Piechocka-Trocha, A., Li, J.Z., Khatri, A., Chu, H.Y., Mgh Covid- Collection, Team Processing, Villani, A.C., Kays, K., Goldberg, M.B., Hacohen, N., Filbin, M.R., Yu, X. G., Walker, B.D., Wesemann, D.R., Larman, H.B., Lederer, J.A., Elledge, S.J., 2020. Viral epitope profiling of COVID-19 patients reveals cross-reactivity and correlates of severity. Science 370.